# Earthquake catalog of induced seismicity recorded during and after stimulation of Enhanced Geothermal System in Helsinki, Finland
(https://doi.org/10.5880/GFZ.4.2.2021.001)

Maria Leonhardt [1], Grzegorz Kwiatek [1], Patricia Martínez-Garzón[1], Pekka Heikkinen[2]

1. Helmholtz Centre Potsdam, GFZ German Research Centre for Geosciences, Section 4.2: Geomechanics and Scientific Drilling, Potsdam, Germany
2. Department of Geosciences and Geography, University of Helsinki, Helsinki, Finland

## 1. Licence



## 2. Citation

**When using the data please cite:**

Leonhardt, M.; Kwiatek, G.; Martínez-Garzòn, P.; Heikkinen, P. (2021): Earthquake catalog of induced seismicity recorded during and after stimulation of Enhanced Geothermal System in Helsinki, Finland. GFZ Data Services. https://doi.org/10.5880/GFZ.4.2.2021.001

**The data are supplementary material to:**

Leonhardt, M., Kwiatek, G., Martínez-Garzón, P., Bohnhoff, M., Saarno, T., Heikkinen, P., & Dresen, G. (2021). Seismicity during and after stimulation of a 6.1 km deep enhanced geothermal system in Helsinki, Finland. Solid Earth, 12(3), 581–594. https://doi.org/10.5194/se-12-581-2021

## Table of contents

# 3. Data Description

The dataset is a high-resolution catalog of seismicity framing the stimulation campaign of a 6.1 km deep Enhanced Geothermal System (EGS) in Helsinki suburban area, Finland. Within the St1 Deep Heat project, a total of 18,160 $m^3$ of fresh water was injected into crystalline rocks during 49 days in summer 2018. The seismicity was monitored by a 12-level seismometer array at ≥2km depth and a seismic network of near-surface borehole sensors surrounding the EGS site. We expanded and refined the original catalog of Kwiatek et al. (2019) including detected seismic events and earthquakes that occurred two month after the end of injection and determining new locations and relocations on the basis of a new velocity model derived from a post-stimulation vertical seismic profiling campaign.

The dataset is supplementary material to the Solid Earth research article of Leonhardt et al. (2021).

## 3.1. Seismic catalog development

The original seismic catalog created during stimulation campaign has been reprocessed by Kwiatek et al. (2019), and included 6,150 located and ~54,000 detected earthquakes.

In first step, this catalog was extended in time to cover the post-stimulation period of 63 days. In the following, we selected best quality 5,456 events that were located during and after the stimulation, and reprocessed them in our study, as discussed in details below. The original catalog of detections was reviewed as well, resulting in 55,707 smaller events detected during stimulation until the 1st of August 2018. Thus, the total seismic catalog presented in this data publication contains 61,163 earthquakes in the period of 112 days. In the following sections we present the development of seismic catalog.

### 3.1.1. Seismic network

Following Kwiatek et al. (2019), the real-time telemetered network monitoring the stimulation campaign was composed of 24 borehole seismographs, fabricated, installed, and operated by Advanced Seismic Instrumentation and Research (www.asirseismic.com). The 12-level borehole array of three-component 15-Hz natural frequency Geospace OMNI-2400 geophones was sampled at 2 kHz and placed at depths of 1.95 to 2.37 km in the *OTN-2* well. Additional 12-station three-component $f_N$ = 4.5 Hz Sunfull PSH geophones sampled at 500 Hz were installed in 0.30- to 1.15-km-deep wells. These surrounded the project site at 0.6- to 8.2-km epicentral distances. These two networks were operating months before the start of stimulation with no event detected in the vicinity of *OTN-3* injection well. Data from these 24 sensors were used in processing of seismic data forming the data publication.

### 3.1.2. Detection catalog

We followed the same approach as presented in Kwiatek et al. (2019). P-wave arrivals unused in locations, but detected using the array located in *OTN-2* well, were further analyzed. Assuming that a small event that is detected solely at the *OTN-2* array must occur in its immediate vicinity, we placed a hypothetical seismic source at the bottom of *OTN-3* where the injection took place. We then calculated travel times of P-waves to the sensors forming the *OTN-2* array, obtaining a particular pattern (offset) of expected P-wave arrivals at these stations. We then scanned the catalog of unused *OTN-2* P-wave arrivals for this particular pattern, and each matching set of detections was attributed to an event occurring in the vicinity of the *OTN-3* well. The magnitude (see section 3.1.5) was calculated assuming that the event occurred at the bottom of the *OTN-3* injection well. This procedure allowed us to enhance the catalog by 55,707 earthquakes.

### 3.1.3. VSP-based velocity model

In original study of Kwiatek et al. (2019), the 1D velocity model based on velocity logs was used. In the study of Leonhardt et al. (2021), the new velocity model was developed from P-wave onset times of calibration shots obtained during a post-injection Vertical Seismic Profiling (VSP) campaign.

The VSP campaign was performed in October 2018 after the end of the stimulation. Overall, 47 calibration shots were performed at 7 shot points located around the injection well *OTN-3* with a maximum distance of less than 8 km. Shot points were prepared with explosives in holes up to 40 m depth. The VSP campaign was monitored by a 17-level vertical chain with 3-components geophones located in the injection well *OTN-3* in a depth between 2.5 km and 4.5 km. In addition, the 12-level vertical geophone chain, used for the stimulation, was also monitoring the VSP shots to cover the depth above 2.5 km.

The 1D velocity model used in Leonhardt et al. (2021) was developed from the data of VSP shot performed close to the OTRA station. This secured that wave propagation ray was nearly vertical between the shot location and seismic arrays. This allowed us to convert travel-path velocities calculated at different sensors forming the array along the *OTN-3* well to interval velocities of the 1D velocity model. For the depths below 4.5 km which was not covered by seismic rays of VSP shots we used information from sonic logs, available depth between 5.1 km and 6.4 km. The velocity model is presented in Fig. 1. Due to a low Signal-to-Noise (S/N) ratio of the VSP data, the S-wave arrival times could not be determined.

The 1D VSP-derived velocity model shows a velocity inversion between 3 and 6 km depth (Fig. 1). The maximum P-wave velocity is 0.15 km $s^{-1}$ larger than the maximum velocity modelled by Kwiatek et al. (2019) where a constant velocity of 6.4 km $s^{-1}$ starting at 3 km depth was assumed. Below the velocity inversion, approximately constant velocity of 6 km $s^{-1}$ is suggested from sonic logs for the updated 1D velocity model (Fig. 1).

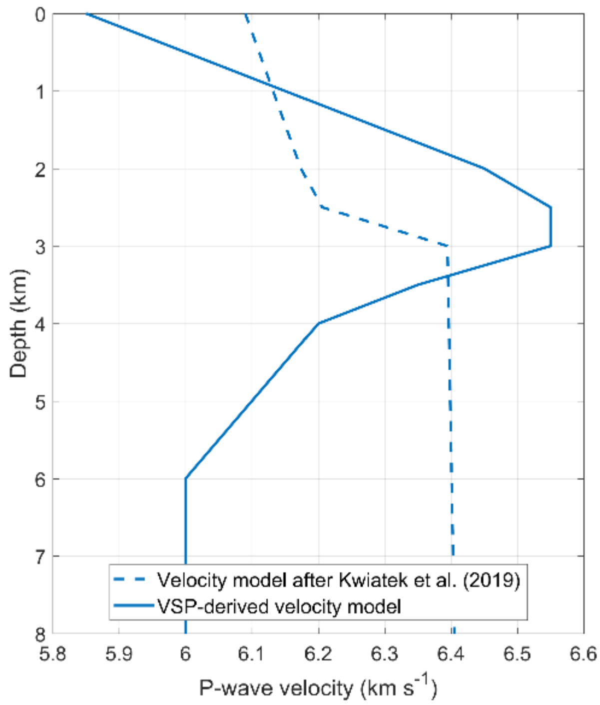


***Figure 1**. Comparison of 1D velocity model developed from VSP profiling (solid line) and the one used in Kwiatek et al. (2019).*

### 3.1.4. Earthquake location and relocation

The sub-catalog of 5,456 events was reprocessed applying the new 1D layered velocity model. Thus, the $V_P/V_S$ ratio had to be optimized by a trial-and-error procedure, as discussed in Leonhardt (2021). We found the optimum $V_P/V_S$ by minimizing the cumulative residual errors of all located events while keeping first induced seismic events close to the injection well *OTN-3*. The optimized $V_P/V_S$ ratio of 1.71 was therefore selected which is similar to that used in Hillers et al. (2020).

The hypocenter locations were estimated using the Equal Differential Time (EDT) method (Zhou, 1994; Font et al., 2004; Lomax, 2005) and the new VSP-derived velocity model. In addition, station corrections were applied. The minimization of travel time residuals:

$$\left|\left|\left(T_j^{th} - T_i^{th}\right) - \left(T_j^{obs} - T_i^{obs}\right)\right|\right|_{L_2} = min, \qquad (1)$$

where $T^{th}$ and $T^{obs}$ are all unique pairs (i,j) of theoretical and observed travel times of P- and S-phases, were resolved using the Simplex algorithm (Nelder and Mead, 1965; Lagarias et al., 1998) . A total of 2,958 reprocessed events were absolute located around the injection well *OTN-3* at an epicentral distance of less than 5 km and at depth of 4.5 to 7 km. The hypocenters of these events were included to the reprocessed and published catalog.

To further refine the quality of hypocenter locations, 2,178 from the 2,958 absolute located events with at least 10 P-wave and 4 S-wave picks were selected and the double-difference relocation technique (hypoDD) was applied using the new VSP-derived velocity model (Waldhauser and Ellsworth, 2000). An iterative least-square inversion was used to minimize residuals of observed and predicted travel time differences for event pairs calculated from the existing P- and S-wave picks of the selected catalog data. The residuals were minimized in ten iterations steps. For the last iteration, the maximum threshold for travel time residuals were set to 0.08 s and the maximum distance between the catalog linked event pairs was defined as 170 m. With the hypoDD method 1,986 events were relocated and thus 91 % of the selected 2,178 events. The residuals of the relocations have a root mean square error of 9 ms. The relocation uncertainties were then assessed using a bootstrap technique (Waldhauser and Ellsworth, 2000; Efron, 1982) leading to relative location precision not exceeding ±52 m for 95 % of the catalog.

### 3.1.5. Basic source characteristics and statistical properties

Local "Helsinki" magnitude $M_{LHEL}$ has been calculated from ground displacement seismograms integrated from ground velocity records (Uski and Tuppurainen, 1996; further updated by Uski et al. (2015) to smaller events). The magnitude was calculated separately on each station (24 sensors) using vertical component seismograms, and then averaged. The moment magnitudes of all events were estimated from local magnitudes $M_{LHEL}$ using formula from Uski et al. (2015). The seismic moment was recalculated from $M_W$ using formula of Hanks and Kanamori (1979).

The magnitude of completeness $M_C$ as well as the *b*-value were calculated assuming a Gutenberg-Richter (GR) power law: $\log_{10} N = a - bM_C$, where *N* is the cumulative number of earthquakes with magnitudes larger than $M_C$. Following the Goodness-of-fit method (Wiemer and Wyss, 2000), the magnitude of completeness and the *b*-value were estimated assuming that the GR power law can fit 98 % of the seismic data.

## 3.2. Seismic catalog properties

The reprocessed seismic catalog covers the time period between 4th of June and 24th of September 2018. The stimulation was performed during the first 49 days. After shut-in of injection, i.e. after 22nd of July 2018 at 15:52 UTC, further 63 days of the post-stimulation time period were monitored.

Overall, 61,163 earthquakes were detected during and after the stimulation. From the 55,707 events that were detected but not further processed, 52,107 detections occurred during the stimulation whereas another 3,600 detections were monitored after the stimulation until 1st of August 2018. From the 5,456 events that were further processed, 4,510 events were monitored during and 946 events were monitored after the end of stimulation.

### 3.2.1. Moment magnitudes

The 55,707 event detections, that were not further located or processed, had moment magnitudes between $M_W = -0.95$ and $M_W = 1.53$. The subset of 2,958 events that were absolute located within the target volume around the injection well *OTN-3* with an epicentral distance of less than 5 km and a depth between 4.5 km and 7 km had moment magnitudes between $M_W = -0.84$ and $M_W = 1.87$. The 213 post-injection events that were absolute located within the target volume around *OTN-3* showed a minimum moment magnitude of $M_W = -0.69$. The largest observed magnitude was $M_W = 1.54$ for the absolute located post-stimulation events. The subset of 1,987 relocated events showed moment magnitudes between $M_W = -0.49$ and $M_W = 1.87$. The 70 relocated post-stimulation events had a minimum magnitude of $M_W \geq -0.07$.

### 3.2.2. Relocated catalog

Figure 2 presents the relocated seismicity which occurred in three spatially separated clusters elongated in southeast (SE) - northwest (NW) direction and centered along the injection well, in good agreement with Kwiatek et al. (2019). Elongation of the clusters in SE-NW direction is sub-parallel to the local maximum horizontal stress $S_H^{max} = 110°$ (Kwiatek et al., 2019). Further details about the relocated seismicity are discussed in Leonhardt et al. (2021).

### 3.2.1. Spatio-temporal characteristics

Figure 3 shows the development of the seismicity with the horizontal distance from injection well *OTN-3*. This shows quick expansion of seismicity in lateral direction (mostly along SE-NW direction) in first two stimulation phases P1-P2 lasting 20 days (cf. Kwiatek et al., 2019), where the injection rates and injection well head pressures were the highest (cf. Kwiatek et al., 2019; Leonhardt et al., 2021). In following stimulation phases P3-P5, the expansion is slower and the seismicity front reaches approx. 400 m horizontal distance from *OTN-3* well. The post-stimulation phase displays no signatures in propagation with scattered seismicity confined to 400 m horizontal distance from *OTN-3* well.

Figure 4 presents the dependence between earthquake depth and local magnitude. The figure marks the three distinct clusters of seismicity (cf. Fig. 2) developed during hydraulic stimulation. Largest seismic events as well as the highest level of seismic activity is observed in the lowermost cluster. This is expected due to expected elevated pore fluid pressures in the direct vicinity of injection activities, suggesting the seismic activity, as well as maximum magnitude is pressure-controlled (cf. discussion in Kwiatek et al., 2019; Bentz et al., 2020; Wang et al., 2020a, 2020b).

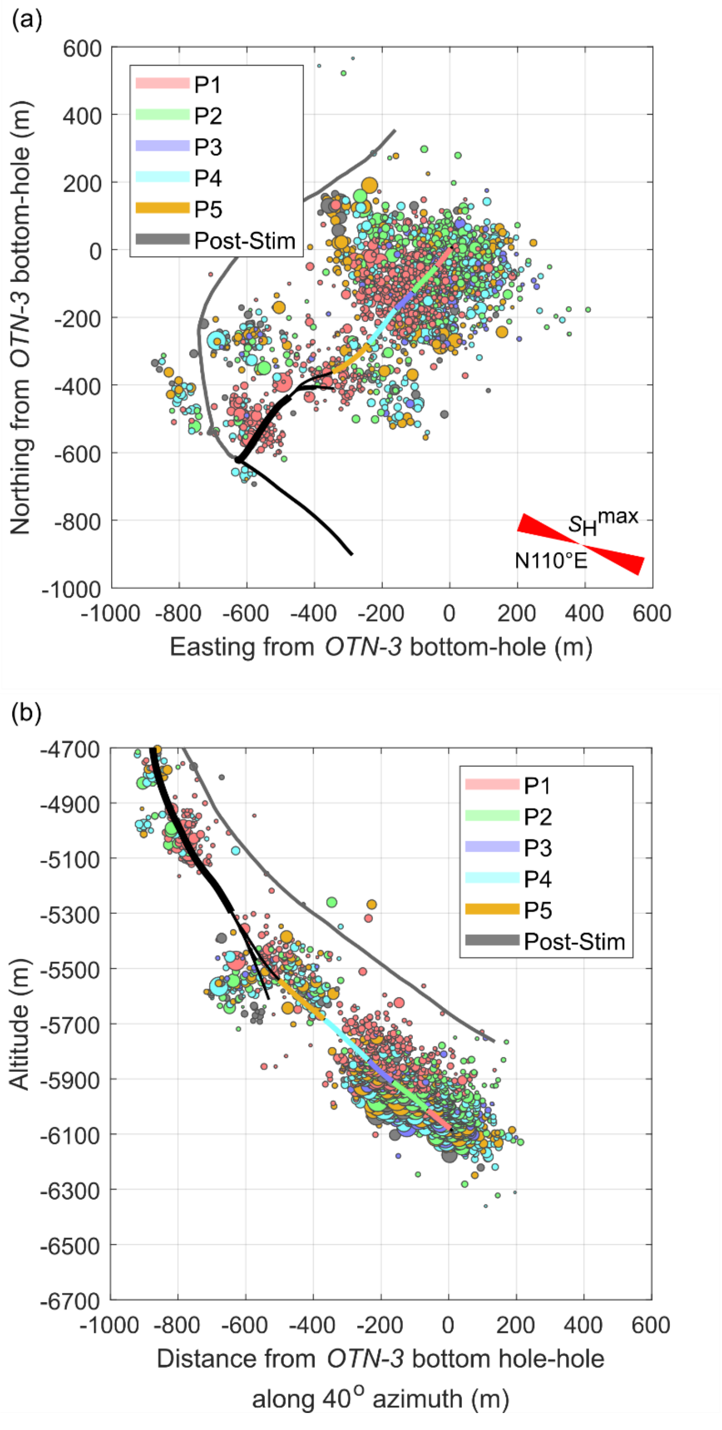


***Figure 2.*** *Hypocenters of relocated events. (a) Map view and (b) SW-NE depth section. The hypocenters are color-coded with the stimulation phases (cf. Kwiatek et al., 2019) and size corresponds to moment magnitude. Relocated seismicity that occurred after the stimulation is represented as grey dots. The five injection stages are marked as color bands along the borehole trace from the bottom of the open-hole toward the casing shoe of the injection well OTN-3 (black). The new OTN-2 well (grey) was drilled in 2019 to 2020 after the stimulation.*

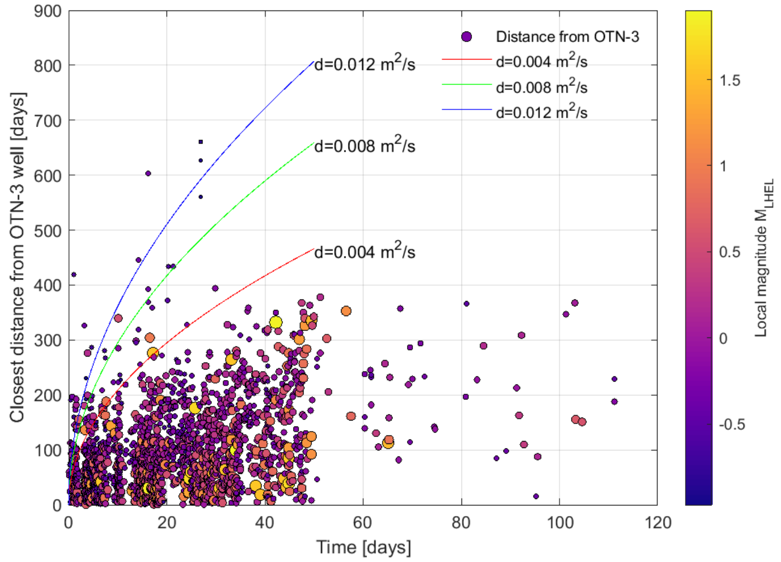


***Figure 3**. Spatial development of the seismicity with time during OTN-3 stimulation (until day 49) and in post-stimulation phase (from day 49). For each event, the distance is calculated as a distance between earthquake epicenter (EASTING, NORTHING) and the coordinate of the OTN-3 well (EASTING, NORTHING) at the depth of earthquake (horizontal distance). The red, blue and green curves represent expected space-time evolution of a fluid pressure perturbation front triggering seismicity assuming that it is solely controlled be scalar fluid pressure diffusion in a homogeneous isotropic medium (e.g. Shapiro et. al., 2020).*

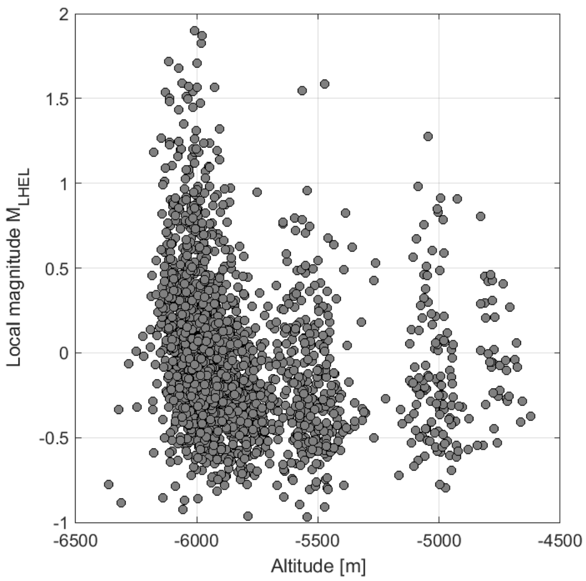


***Figure 4**. Dependence between earthquake depth (here presented as altitude a.s.l.) and local magnitude.*

### 3.2.2. Gutenberg-Richter distribution

The catalog combining locations and detections displays $b = 1.25$ with magnitude of completeness $M_C = -1.10$ (Figure 5). Above $M_{LHEL}$ 1.5 the statistically significant roll-off is visible which was attributed to either geometrical constraint on pre-existing fracture network or limitation to fault strength (cf. Kwiatek at al., 2019). We note that although the magnitude of completeness of the full catalog is $M_C = -1.10$ assuming the goodness-of-fit criteria, the day-night cycles and associated anthropogenic noises visibly reduces the completeness by approx. 0.2 (cf. Figure 2 in Kwiatek et al. (2019) where day-night cycle is clearly visible).

We note processing of events with $M_{LHEL}$ < -0.7 should be performed with caution. In a pending study (G. Kwiatek – pers. comm.) we note local magnitude estimates of small events with $M_{LHEL}$ < -0.7 are affected by high-frequency noises above 60 Hz (multiple resonance peaks) observed on sensors forming the vertical array in *OTN-2* well. The origin of these additive noises has been correlated to technological activities at the injection site, with the most likely noise source attributed to the high-performance injection pumps, as the noise seem to be correlation to injection rates. As recordings from *OTN-2* arrays are used to calculate local magnitude of smaller events that are not detected using the sensors close to the surface, and the local magnitude is calculated from integrated ground displacement seismograms which further emphasize the (temporary varying and resonant) noises, we observe bias in estimates of $M_{LHEL}$ for $M_{LHEL}$ < -0.7. We identified this may lead to potential problems while analyzing statistical properties of induced seismicity such as magnitude correlations and or inter-event time statistics, to name a few. We suggest $M_C$ = -0.7 as a reasonably safe magnitude threshold that is not affected by noises originating from technological activity and day-night cycles. The subject is a topic of pending study (G. Kwiatek – pers. comm.) and this document and associated dataset will be updated accordingly when new information becomes available.

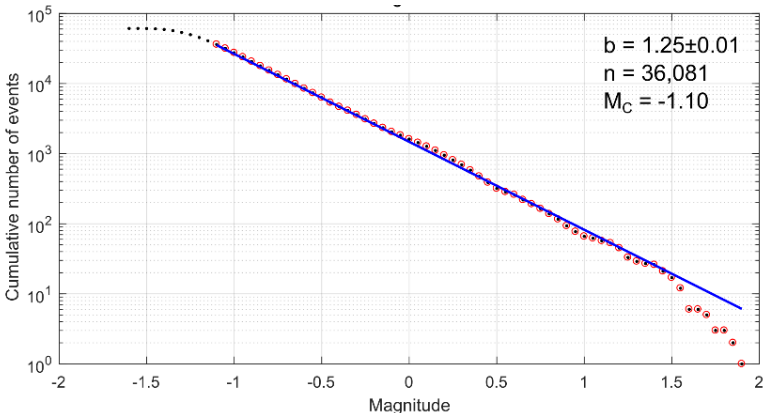


***Figure 5**. Magnitude-frequency relation for the entire seismic catalog analyzed in Leonhardt et al. (2021).*

# 4. File description

2021-001_Leonhardt-et-al_data_v1.csv is the seismic catalog. For located events, the catalog contains origin times, local as well as moment magnitudes, absolute locations in local Cartesian coordinate system and for relocated events also the double-difference relocated locations in local Cartesian coordinate system. The fault plane solutions (strike, dip and rake) with associated uncertainties of estimated focal mechanisms are also included in the data catalog.

## 4.1. File naming convention

2021-001_Leonhardt-et-al_data_v1.csv:

Version 1 (2020.01.25): Initial release of the catalog as processed and presented in Leonhardt et al. (2021).

## 4.2. Description of data table

File 2021-001_Leonhardt-et-al_data_v1.csv contains the seismic catalog in form of a data table structured as follows:

| Column header | unit | Description |
|---|---|---|
| ID | | ID number of event |
| Classification of event | | **Class = 1:** event is within the defined target volume (at epicentral distance < 5 km around *OTN-3* and at depth of 4.5 to 7 km) after absolute locating the event<br>**Class = 2**: event is outside of the target volume after absolute locating the event<br>**Class = 3**: detection with assumed locations close to *OTN-3* (see section 3.1.2), ID = 0 |
| Datenumber | | **integer part** = day since year 0,<br>**fractional part** = time within one day, e.g. 0.25 corresponds to 6am, 0.75 to 6pm UTC |
| Year | | UTC time |
| Month | | UTC time |
| Day | | UTC time |
| Hour | | UTC time |
| Minute | | UTC time |
| Second | | UTC time |
| $M_{\mathrm{LHEL}}$ | | Local "Helsinki" magnitude $M_{\mathrm{LHEL}}$ |
| $M_{\mathrm{W}}$ | | Moment magnitude $M_{\mathrm{W}}$ |
| abs. location easting | meters | Hypocenter easting of absolute location in local Cartesian coordinate system (ETRS89 / GK25FIN coordinate system) |
| abs. location northing | meters | Hypocenter northing of absolute location in local Cartesian coordinate system (ETRS89 / GK25FIN coordinate system) |
| abs. location altitude | meters | Hypocenter altitude of absolute location with mean see level corresponding to 0 [m] |
| relocation easting | meters | Hypocenter easting of relocation in local Cartesian coordinate system (ETRS89 / GK25FIN coordinate system) |
| relocation northing | meters | Hypocenter northing of relocation in local Cartesian coordinate system (ETRS89 / GK25FIN coordinate system) |
| relocation altitude | meters | Hypocenter altitude of relocation in local Cartesian coordinate system with mean see level corresponding to 0 [m] |
| FPS-1 Strike | degree | Strike of nodal plane from focal mechanism estimated with *HASH* (Hardebeck and Shearer, 2002); FPS =Fault Plane Solution |
| FPS-1 Dip | degree | Dip of nodal plane from focal mechanism estimated with *HASH* (Hardebeck and Shearer, 2002) |
| FPS-1 Rake | degree | Rake of nodal plane from focal mechanism estimated with *HASH* (Hardebeck and Shearer, 2002) |
| FPS-2 Strike | degree | Strike of 2$^{nd}$ estimated nodal plane based on *HASH* output |
| FPS-2 Dip | degree | Dip of 2$^{nd}$ estimated nodal plane based on *HASH* output |
| FPS-2 Rake | degree | Rake of 2$^{nd}$ estimated nodal plane based on *HASH* output |
| RMS | degree | Root mean square fault plane uncertainty of estimated focal mechanisms (≤ given number) |

## 5. References


Bentz, S., Kwiatek, G., Martínez-Garzón, P., Bohnhoff, M., and Dresen, G.: Seismic moment evolution duringhydraulic stimulations, Geophysical Research Letters, 47, e2019GL086185, https://doi.org/10.1029/2019GL086185, 2020.

Efron, B.: The jackknife, the bootstrap, and other resampling plans, Siam, https://doi.org/10.1137/1.9781611970319, 1982.

Font, Y., Kao, H., Lallemand, S., Liu, C.-S., and Chiao, L.-Y.: Hypocentre determination offshore of eastern Taiwan using the maximum intersection method, Geophysical Journal International, 158, 655–675, https://doi.org/10.1111/j.1365-246X.2004.02317.x, 2004.

Hanks, T.C. and Kanamori, H.: A moment magnitude scale, Journal of Geophysical Research: Solid Earth, 84, 2348–2350, https://doi.org/10.1029/JB084iB05p02348, 1979.

Hardebeck, J. and Shearer, P.: A new method for determining first-motion focal mechanisms, Bulletin of the Seismological Society of America, 92, 2264–2276, https://doi.org/10.1785/0120010200, 2002.

Hillers, G., Vuorinen, T., Uski, M., Kortström, J., Mäntyniemi, P., Tiira, T., Malin, P., and Saarno, T.: The 2018 geothermal reservoir stimulation in Espoo/Helsinki, Southern Finland: Seismic network anatomy and data features, Seismological Research Letters, 91 (2A), 770–786, https://doi.org/10.1785/0220190253, 2020.

Kwiatek, G., Saarno, T., Ader, T., Bluemle, F., Bohnhoff, M., Chendorain, M., Dresen, G., Heikkinen, P., Kukkonen, I., Leary, P., Leonhardt, M., Malin, P., Martínez-Garzón, P., Passmore, K., Passmore, P., Valenzuela, S., and Wollin, C.: Controlling fluid-induced seismicity during a 6.1-km-deep geothermal stimulation in Finland, Science Advances, 5, eaav7224, https://doi.org/10.1126/sciadv.aav7224, 2019.

Lagarias, J.C., Reeds, J.A., Wright, M.H., and Wright, P.E.: Convergence properties of the Nelder--Mead simplex method in low dimensions, SIAM J. Optim., 9, 112–147, https://doi.org/10.1137/S1052623496303470, 1998.

Leonhardt, M., Kwiatek, G., Martínez-Garzón, P., Bohnhoff, M., Saarno, T., Heikkinen, P., & Dresen, G.: Seismicity during and after stimulation of a 6.1 km deep enhanced geothermal system in Helsinki, Finland. Solid Earth, 12(3), 581–594. https://doi.org/10.5194/se-12-581-2021, 2021.

Lomax, A.: A reanalysis of the hypocentral location and related observations for the great 1906 California earthquake, Bulletin of the Seismological Society of America, 95, 861–877, https://doi.org/10.1785/0120040141, 2005.

Nelder, J.A. and Mead, R.: A simplex method for function minimization, The Computer Journal, 7, 308–313, https://doi.org/10.1093/comjnl/7.4.308, 1965.

Shapiro, S. A., Rothert, E., Rath, V., and Rindschwentner, J.: Characterization of fluid transport properties of reservoirs using induced microseismicity, Geophysics, 67(1), 212–220, https://doi.org/10.1190/1.1451597, 2020.

Uski, M. and Tuppurainen, A.: A new local magnitude scale for the Finnish seismic network, Tectonophysics, 261, 23–37, https://doi.org/10.1016/0040-1951(96)00054-6, 1996.

Uski, M., Lund, B., and Oinonen, K.: Scaling relations for homogeneous moment based magnitude, in: Evaluating seismic hazard for the Hanhikivi nuclear power plant site. Seismological characteristics of the seismic source areas, attenuation of seismic signal, and probabilistic analysis of seismic hazard, edited by: Saari, J., Lund, B., Malm, M., Mäntyniemi, P., Oinonen, K., Tiira, T., Uski, M., and Vuorinen, T., (Report NE-4459, ÅF-Consult Ltd.), 125 pp., 2015.

Waldhauser, F. and Ellsworth, W.L.: A double-difference earthquake location algorithm: Method and application to the Northern Hayward Fault, California, Bulletin of the Seismological Society of America, 90, 1353–1368, https://doi.org/10.1785/0120000006, 2000.

Wang, L., Kwiatek, G., Rybacki, E., Bohnhoff, M., and Dresen, G.: Injection-induced seismic moment release and laboratory fault slip: Implications for fluid-induced seismicity, Geophysical Research Letters, 47, e2020GL089576, https://doi.org/10.1029/2020GL089576, 2020a.

Wang, L., Kwiatek, G., Rybacki, E., Bonnelye, A., Bohnhoff, M., and Dresen, G.: Laboratory study on fluid-induced fault slip behavior: The role of fluid pressurization rate, Geophysical Research Letters, 47, e2019GL086627, https://doi.org/10.1029/2019GL086627, 2020b.

Wiemer, S. and Wyss, M.: Minimum magnitude of completeness in earthquake catalogs: Examples from Alaska, the Western United States & Japan, Bull. Seismol. Soc. Am, 90, 859–869, https://doi.org/10.1785/0119990114, 2000.

Zhou, H.: Rapid three-dimensional hypocentral determination using a master station method, Journal of Geophysical Research: Solid Earth, 99, 15439–15455, https://doi.org/10.1029/94JB00934, 1994.